



Inducing intermittency in the inverse cascade of two-dimensional turbulence by a fractal forcing

George Sofiadis  and Ioannis E. Sarris 

Department of Mechanical Engineering, University of West Attica, 250 Thivon & P. Ralli Street, Egaleo, GR-122 44 Athens, Greece

Alexandros Alexakis ^{*}

Laboratoire de Physique de l'Ecole Normale Supérieure, ENS, Université PSL, CNRS, Sorbonne Université, Université de Paris, F-75005 Paris, France



(Received 7 June 2022; accepted 6 February 2023; published 24 February 2023)

We demonstrate that, as in the forward cascade of three-dimensional turbulence that displays intermittency (a lack of self-similarity) due to the concentration of energy dissipation in a small set of fractal dimension less than three, the inverse cascade of two-dimensional turbulence can also display a lack of self-similarity and intermittency if the energy injection is constrained in a fractal set of dimension less than two. A series of numerical simulations of two-dimensional turbulence are examined, using different forcing functions of the same forcing length scale but different fractal dimension D that varies from the classical $D = 2$ case to the point vortex case $D = 0$. It is shown that as the fractal dimension of the forcing is decreased from $D = 2$, the self-similarity is lost and intermittency appears. The present model thus provides a unique example that intermittency is controlled and can thus shed light and provide test beds for multifractal models of turbulence.

DOI: [10.1103/PhysRevFluids.8.024607](https://doi.org/10.1103/PhysRevFluids.8.024607)

I. INTRODUCTION

Turbulence is pervasive in natural and industrial flows. In his first statistical description of turbulence, Kolmogorov [1] argued that the energy in turbulent flows cascades to smaller and smaller scales in such a way that there is a constant flux of energy from the large scales where energy is injected to the small viscous scales where energy is dissipated. Assuming further that this process is self-similar leads to the prediction that the different moments of velocity differences

$$S_p(r) \equiv \left\langle \left| \frac{\mathbf{r}}{r} \cdot [\mathbf{u}(\mathbf{x} + \mathbf{r}) - \mathbf{u}(\mathbf{x})] \right|^p \right\rangle \quad (1)$$

separated by a distance $r = |\mathbf{r}|$ scale as $S_p \propto r^{p/3}$, with the case $p = 3$ being an exact result [without the absolute value in Eq. (1)]. There is a mass of evidence, however, from the past years that this result is not exact; self-similarity is broken and the powers of velocity differences scale with different exponents $S_p(r) \propto r^{\zeta_p}$ where $\zeta_p \neq p/3$. This breaking of self-similarity is referred to as intermittency. It appears because as the cascade develops towards smaller scales, energy is concentrated in a set that occupies a smaller and smaller fraction of the domain volume so that finally energy dissipation is concentrated in a fractal set of dimension smaller than three [2]. The modern theory of turbulence attempts to understand quantitatively the origin of intermittency and predict these exponents [3,4].

*alexakis@phys.ens.fr

TABLE I. Resolution N , scale separation $\lambda = L/\ell_f$, and hypoviscous Reynolds number Re_α .

| N | 512 | 1024 | 2048 | 4096 |
|--------------------|-------------------|-------------------|-------------------|-------------------|
| λ | 16 | 32 | 64 | 128 |
| Re_α | 4.4×10^4 | 2.8×10^5 | 1.8×10^6 | 1.1×10^7 |

In two dimensions, on the other hand, due to the presence of a second invariant, enstrophy, the energy cascades in an inverse way from small to large scales [5]. This behavior was first predicted by Kraichnan-Leith-Batchelor (KLB) theory (see Refs. [6–8]). What was equally interesting was that the inverse cascade of energy in two dimensions is in fact self-similar so that all moments of velocity differences scale with r with exponents $\zeta_p = p/3$ [9]. This is explained by the fact that larger eddies extract energy from an ensemble of smaller eddies averaging out this way any extreme events. This behavior, as we argue in this paper, does not always have to be the case. If the energy injection in two-dimensional turbulence is not space filling but is restricted in a set of dimension D smaller than two, then as energy moves up in scale it can occupy a larger and larger area fraction so that only at large scales is it concentrated in a two-dimensional set.

Fractal forcing has been employed extensively in three-dimensional turbulence with the use of fractal grids in simulations and wind tunnel experiments in order to enhance turbulence [10–14]. In nature, atmospheric and oceanic flows driven by winds over rough topography [15,16] resemble two-dimensional turbulence driven by a fractal forcing. Furthermore, quasi-two-dimensional flows are believed to transition to an inverse cascade in a critical manner [4]. In such flows the energy injected in the two-dimensional manifold appears in a set of smaller dimension occupying a fraction of the domain area that approaches zero as criticality is approached [17,18].

In this paper we show using an extensive set of numerical simulations that indeed intermittency can appear in the inverse cascade of energy when the energy-injection mechanism is restricted to a set of fractal dimension $D < 2$. This model not only gives different insights in two-dimensional turbulence but also provides a unique example that intermittency can be controlled and can thus provide test beds for multifractal models of turbulence.

II. NUMERICAL SIMULATIONS

We begin by considering the incompressible flow in a double periodic square domain of side $2\pi L$. In terms of the vorticity ω the two-dimensional Navier-Stokes equation can be written as

$$\partial_t \omega + \mathbf{u} \cdot \nabla \omega = \nu \nabla^2 \omega + \alpha \nabla^{-2} \omega + f_\omega \quad (2)$$

where the velocity \mathbf{u} is linked to ω by $\omega = \nabla \times \mathbf{u}$, ν is the viscosity, and α is a hypoviscosity used to absorb energy arriving at the largest scales at a rate $\epsilon_\alpha = \alpha \langle |\nabla^{-1} \mathbf{u}|^2 \rangle$. The curl of the forcing is given by f_ω that injects energy at a rate ϵ at a length scale ℓ_f . Given the functional form of f_ω , there are three independent nondimensional control numbers: the Reynolds number $\text{Re} = \epsilon^{1/3} \ell_f^{4/3} / \nu$, the hypoviscous Reynolds number $\text{Re}_\alpha = \epsilon^{1/3} \ell_f^{-8/3} / \alpha$, and the domain to forcing-scale ratio $\lambda = L/\ell_f$. This system of equations was solved numerically using the pseudospectral code GHOST [19] with $2/3$ dealiasing and second-order Runge-Kutta method for the time advancement. Since we are interested in the inverse cascade the Reynolds number was kept fixed to a small value $\text{Re} = 10$. This value of Re is sufficiently large to allow for the development of the inverse cascade but suppresses the forward enstrophy cascade and any intermittency related to it. As a result the smallest scales in the system are given by ℓ_f and energy in these scales is concentrated close to the forcing. The hypoviscous Reynolds number Re_α was set to $\text{Re}_\alpha = 20\lambda^{8/3}$ so that the large-scale dissipation length scale ℓ_α remains fixed and close to the domain size $\ell_\alpha \simeq L$. Five different resolutions N were used, varying λ as given in Table I.



FIG. 1. Demonstration of how a fractal set of box-counting dimension $1/2$ is formed. At every step (down) the initial set is split into four equal subsets out of which subsets 1 and 3 are disregarded. After N steps there are $n = 2^N$ sets left of length $\ell = L/4^N$. Therefore the number of “boxes” of length ℓ required to cover the remaining sets are $n = (L/\ell)^D$ with $D = 1/2$.

Finally, five different forcing functions of different fractal dimension D are considered. The first one corresponding to $D = 2$ is the classical random forcing where all Fourier modes of wave vectors \mathbf{k} satisfying $|\mathbf{k}| \simeq 1/\ell_f$ are forced with random phases. The $D = 1$ forcing corresponds to four vertical and four horizontal vortex lines with Gaussian profiles of width ℓ_f randomly placed in the domain. Similarly, $D = 0$ corresponds to eight point vortices with a Gaussian profile of width ℓ_f randomly placed in the domain. The $D = 3/2$ and $D = 1/2$ correspond to Cantor sets that are constructed as follows. For $D = 3/2$ a dense set of horizontal and vertical vortex lines are uniformly placed in the domain. This set is split into four equal subsets from which subsets one and three are removed. The remaining sets are then split again in four from which again subsets one and three are removed and so on, as demonstrated in Fig. 1, until no further splitting can be done. The resulting box-counting dimension is $D = 3/2$ [20,21]. For $D = 1/2$ we start with point vortices placed along one vertical and one horizontal line and we follow the same procedure leading this time to a box-counting dimension $D = 1/2$.

For all forcing functions the forcing length scale ℓ_f was fixed so that energy injection was around a similar wave number $k_f \simeq 1/\ell_f$. Furthermore, in all cases the amplitude of the forcing function was varied, randomly delta correlated in time, fixing thus the energy injection rate ϵ . In addition, the forcing pattern moved in space following a slow random walk. The forcing function thus is written as

$$f_w = A(t)f_D([x - x_*(t)]/\ell_f), \quad (3)$$

where $f_D(x)$ gives the functional form $A(t)$ random and delta correlated and $x_*(t)$ follows a random walk. The random displacement in space makes at long timescales all points in space to be equivalent. The timescale of the random displacement is smaller than the eddy turnover time so that the forcing appears fixed within the survival time of the eddies. We note that although the instantaneous forcing is very inhomogeneous, homogeneity is recovered in a statistical sense only when averaging over very long timescales where the random shifting has led the forcing to cover the hole domain. Inhomogeneity and nonsteadiness have been claimed to alter the properties of the cascade even in three-dimensional turbulence in Ref. [22] where a fractal forcing was also used.

A color plot of a realization of the forcing functions for the five forcing functions is shown in the upper panels of Fig. 2. For this figure we used the smallest λ (largest ℓ_f) so that the point vortices in the left panel are clearly visible.

III. RESULTS

All forcing functions lead to an inverse cascade of energy marked by an energy spectrum close to $k^{-5/3}$ (left panel of Fig. 3) and a negative flux of energy

$$\Pi(k) = \langle \mathbf{u}_k^< \cdot (\mathbf{u} \cdot \nabla \mathbf{u}) \rangle \quad (4)$$

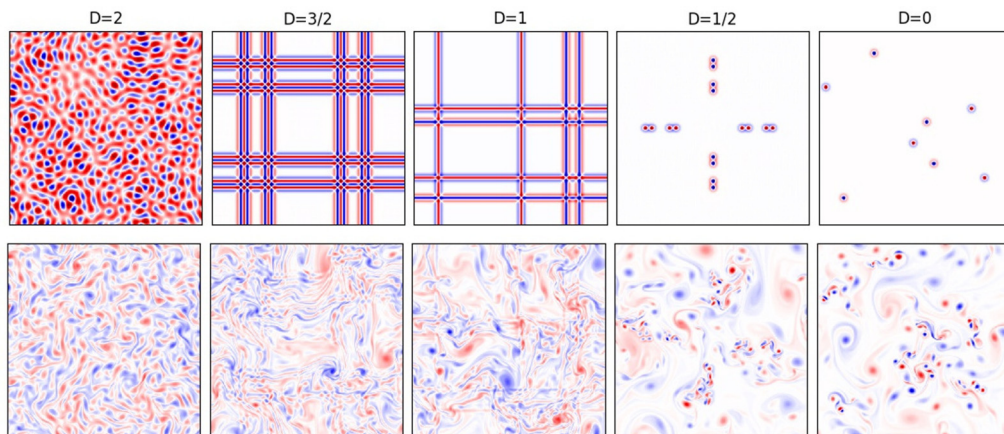


FIG. 2. Top panels: Random forcing function for different dimension D at resolution $N = 512$. Lower panels: Vorticity of the flow for the same cases as above at steady state.

(where \mathbf{u}_k^\leq indicates the field \mathbf{u} filtered so that only wave numbers with $|\mathbf{k}| \leq k$ are kept) shown in the lower panel of Fig. 3. The flux is negative, approximately constant in the range $0.01k_f < k < 0.2k_f$.

Although all five cases have an inverse cascade, they do not have the same turbulent statistical behavior. This can already be seen in the vorticity plots shown in the lower panels of Fig. 2. Turbulence, marked by intense vorticity regions, is uniformly spread in the domain for the $D = 2$ case but as D is decreased intense vorticity regions occupy a smaller area fraction but with a larger intensity. This behavior can be seen to be more pronounced in the high-resolution cases $N = 4096$ shown in Fig. 4 where the color plots of $\tanh(0.01\omega)$ are displayed for the two extreme cases $D = 2$ and $D = 0$. In the $D = 2$ no particular structure can be identified other than some large-scale vortices. In the $D = 0$ case one can easily see clusters of vortices of different sizes and at the same time regions with almost no activity. Clearly, the two flows differ.

In order to quantify this observation we plot in Fig. 5 the probability distribution function (pdf) of velocity differences for all cases for different values of r starting from the largest $r = L/4$ to the forcing scale $r = L/128 = \ell_f$. In the $D = 2$ case the pdfs are close to Gaussian for all examined r . Furthermore, no significant change is observed as r is varied, i.e., they are self-similar. For smaller

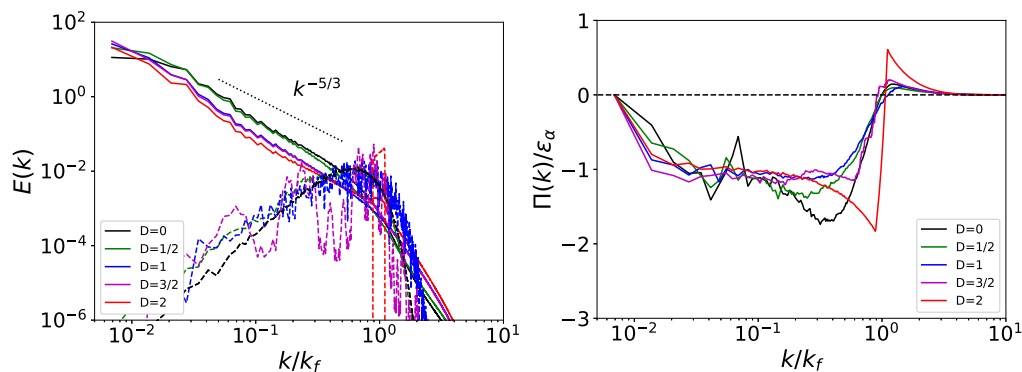


FIG. 3. Left: Energy spectra for the highest-resolution runs. The dashed lines give the forcing spectrum. The straight dotted line gives the $k^{-5/3}$ scaling. Right: Energy flux for the same cases.

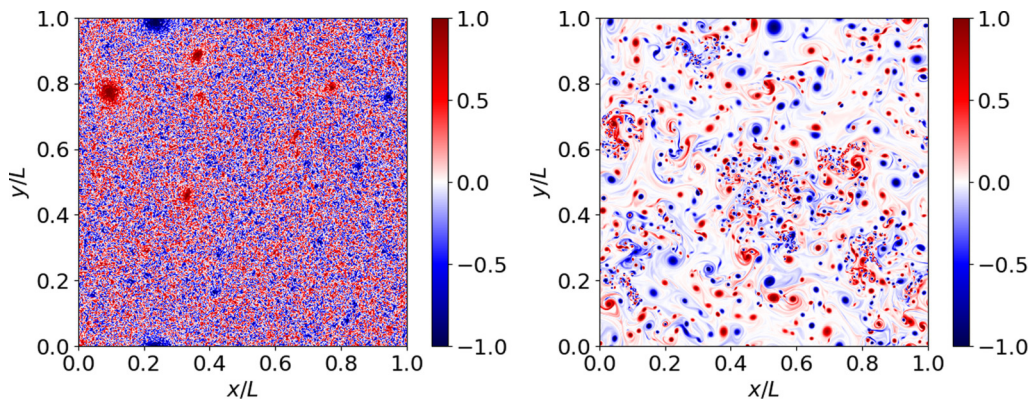


FIG. 4. The panels show $\tanh(0.01\omega)$ obtained from simulations at steady state at the highest resolution $N = 4096$ for fractal forcing dimension $D = 2$ (left) and $D = 0$ (right). Despite all flows being forced at the same length scale and with the same energy injection rate, the resulting structures are visibly different.

values of D , on the other hand, the pdfs deviate from the Gaussian distribution having larger tails. Most importantly, as smaller values of r are considered, the deviations from Gaussianity become stronger with distributions more peaked and with stronger tails. In other words, self-similarity is lost. The bottom panel shows the area fraction of points that have $|\delta u(r)|$ larger than the variance $\sigma_u = S_2(r)^{1/2}$ as a function of r showing that the area fraction is decreasing with L/r , indicating

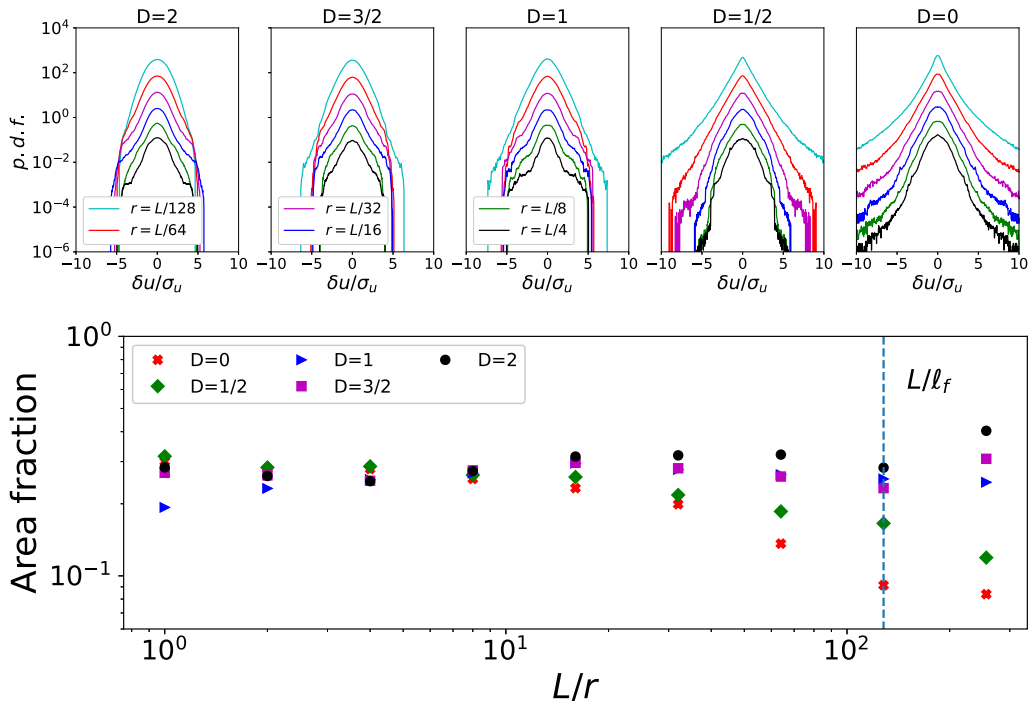


FIG. 5. Top: The probability distribution function of $\delta u(r)$ normalized by its variance $\sigma_u = S_2(r)^{1/2}$ for different values of r and for different values of D . The curves have been shifted vertically for clarity. Bottom: Area fraction of points with $\delta u(r) > \sigma_u$ as a function of r for all D .

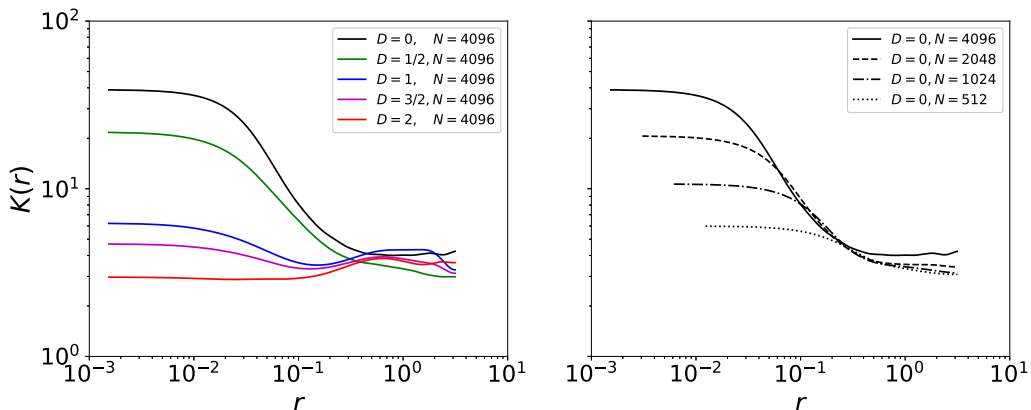


FIG. 6. The left panel shows $K(r)$ for the flows at highest λ for the five different forcing functions. The right panel shows $K(r)$ for $D = 0$ and four different values of λ .

that the breaking of self-similarity is linked to the fact that intense regions occupy a smaller area fraction as smaller scales are examined.

A quantitative way to measure this lack of self-similarity is to measure the kurtosis $K(r) = S_4(r)/S_2^2(r)$. Kurtosis gives a measure of how heavy tailed is the distribution of δu . $K(r) = 3$ corresponds to a Gaussian distributed field while larger values correspond to fields of wider distribution. If the distribution is self-similar, $K(r)$ will be independent of r . In Fig. 6 we plot the kurtosis for different cases. The top panel shows $K(r)$ for the flows at highest $\lambda = 128$ (highest resolution) for the five different forcing functions. For $D = 2$, $K(r)$ is almost flat and close to 3, indicating that δu follows a self-similar, nearly Gaussian distribution. As the dimension of the forcing is decreased, $K(r)$ takes larger and larger values in the small r range, with the $D = 0$ case having more than an order of magnitude larger $K(\ell_f)$ than a Gaussian field. The lower panel shows the case $D = 0$ for the different values of λ . As λ and Re_α are increased, the non-self-similar behavior extends to a larger range of r with the deviation from Gaussianity increasing. Therefore this amounts to a phenomenon that persists and extends as a larger-scale separation between the forcing scale and the dissipation scale is achieved. This implies that in the limit of large Re_α and λ new power laws can form as the flow statistics transition from the highly intermittent behavior at the forcing scale ℓ_f to the nearly Gaussian statistics at the box scale L .

To test this possibility, in Fig. 7 we plot $S_p(r)^{1/p}$ up to order $p = 6$ for the different flows. For all D the scaling $S_3^{1/3}(r) \propto r^{1/3}$ (indicated by the orange dashed line) appears to be reasonably satisfied in a range of scales $r_{\min} < r < r_{\max}$ (inertial range) marked by the vertical dotted lines. Furthermore, for the $D = 2$ case all structure functions appear to also satisfy $S_p^{1/p}(r) \propto S_3^{1/3}(r)$, demonstrating self-similarity. This is no longer the case, however, for smaller values of D . As D is decreased, the slopes of $S_p^{1/p}(r)$ for larger values of p deviate from the $r^{1/3}$ scaling and appear to become less steep, indicating an absence of self-similarity.

The deviation from self-similarity can be measured by calculating the exponents ζ_p . The fitting range for these exponents is rather small but we note that as Fig. 6 demonstrates this range will increase as larger domains are examined. We measured the exponents by using the extended self-similarity assumption [23] that extends the range that a power-law behavior is observed. In the extended self-similarity method $S_p(r)$ is fitted as $S_p(r) \propto S_3(r)^{\zeta'_p}$ instead of $S_p(r) \propto r^{\zeta_p}$. Assuming the theoretically predicted linear scaling of the third moment $S_3(r) \propto r$, one then obtains $\zeta_p = \zeta'_p$. The lower panels of Fig. 7 show $S_p^{1/p}(r)$ plotted as a function of $S_3^{1/3}(r)$ where it has been normalized by $S_3^{1/3}(r)$ to intensify the differences.

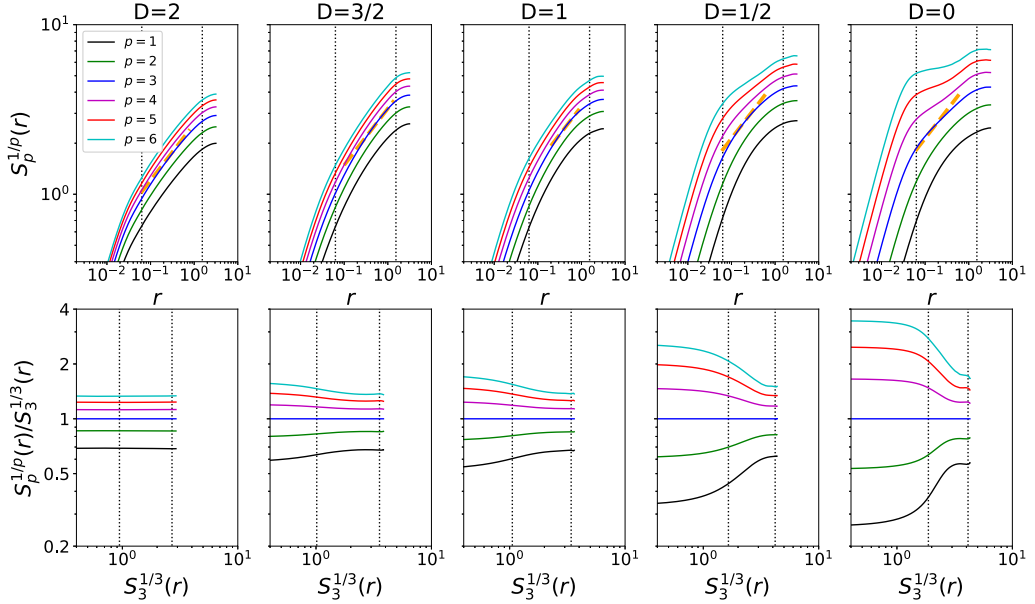


FIG. 7. Top: Structure functions $S_p^{1/p}(r)$ for $p = 1$ to $p = 6$ for all cases. The orange dashed line indicates the $S_p^{1/p} \propto r^{1/3}$ scaling predicted by self-similarity. The vertical dotted lines indicate r_{\min} and r_{\max} that mark the range of the inertial scales where the scaling $S_3^{1/3} \propto r^{1/3}$ appears reasonable. Bottom: Same structure functions normalized by $S_3^{1/3}(r)$ and plotted as a function of $S_3^{1/3}(r)$. The vertical dotted lines correspond to the same lines as the top panel marking $S_3^{1/3}(r_{\min})$ and $S_3^{1/3}(r_{\max})$.

The measured exponents up to $p = 6$ are shown in Fig. 8. For $D = 2$ the exponents follow the linear scaling $\zeta_p = p/3$. As D is decreased, the exponents with $p < 3$ increase while exponents with $p > 3$ decrease. The flow thus becomes more intermittent as D is decreased with the high-order moments being dominated by a few but strong events in the tail of the distribution. In particular,

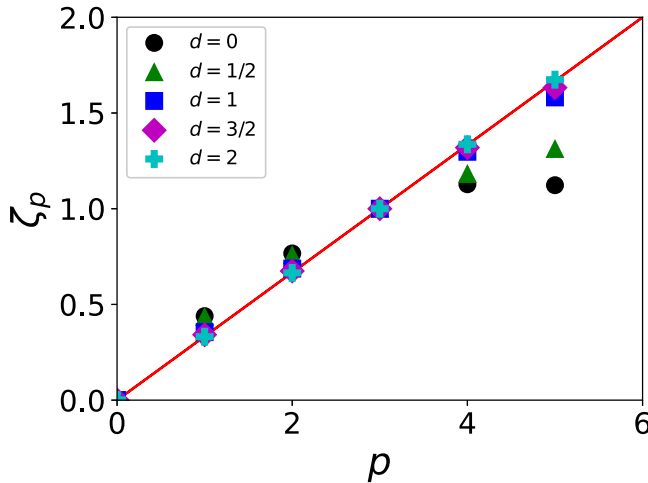


FIG. 8. Scaling exponents ζ_p measured using the extended self-similarity method.

for $D = 0$ the exponents appear to become almost constant as large values of p are approached, something that has to be verified however with larger resolutions and larger values of p .

IV. CONCLUSIONS

In this paper we have shown that the inverse cascade of energy can display intermittent features provided that the forcing function injects energy in a fractal set of dimension smaller than two. Intermittency is demonstrated by long tails in the distribution of the velocity differences at small scales caused by the forcing, that as larger scales are approached they flatten out, becoming closer to Gaussian. This behavior was shown to persist as larger domains (larger λ) are considered. Most importantly, it is shown that the strength of intermittency caused by the fractal forcing is sensitive on its dimension and thus it provides a way to create a cascade for which the intermittency can be varied from self-similar to strongly intermittent. The overall picture that emerges is that larger eddies that occupy a certain area fraction are forced by smaller eddies that occupy a smaller area fraction that themselves are forced by even smaller eddies occupying an even smaller area fraction and so on up to the forcing scale (to paraphrase Richardson's poem). There is thus a non-self-similar cascade process that connects the strongly intermittent forced scales to the Gaussian large scales. Given the simplicity of the present model, ideas about the behavior and origin of intermittency can thus be put in the test using it.

There are thus various limitations of the present results that we would like to discuss. Although, the present results demonstrated the existence of intermittency in 2D flows when fractally forced, we have not examined how universal are these results (given the dimensionality of the forcing). In this work we have used a particular type of fractal forcing. However, the fractal dimension alone does describe all the geometrical properties of the forcing and other geometrical parameters as well as properties of its time evolution can also become important. Various extensions of it can thus be considered in order to identify the key ingredients besides the dimension, that determine the statistical properties of the resulting flows. For example, in the present study the pattern of the forcing moved is space as a slow random walk. As such, large eddies that sweep through the forcing location lead to the generation of a streak of forcing-scale size eddies instead of a single eddy. This behavior could be altered if the random shifting of the forcing is faster or if the location of the forcing moves with the flow. Such alterations in the forcing can increase or decrease the number of eddies generated by the forcing and change the resulting statistics. Another possible variation of the present model is to change the monofractality of the forcing. Here, we employed only monofractal forcing. Bifractal or multifractal forcing can also be considered by adding with appropriate weight different fractal forcing functions. This could lead to an intermittent behavior that is closer to the three-dimensional cascade.

Another aspect that should be further investigated is the role of Re and Re_σ . Here, we limited ourselves to low Re values. It would be interesting to investigate if the present results persist as Re is increased. Also, the effect of hypoviscosity used in this work should also be investigated examining larger or smaller powers of the inverse Laplacian.

Of course, although numerical simulations are invaluable at this state, a theoretical framework that will lead to clear predictions about fractally forced two-dimensional turbulence is still missing. Furthermore, the realization of laboratory experiments of two-dimensional turbulence forced by fractal forcing (as, for example, stirring with thin rods) would be very useful.

Finally, one cannot help but wonder how a fractal forcing can affect intermittency properties in three-dimensional turbulence.

[1] A. N. Kolmogorov, The local structure of turbulence in incompressible viscous fluid for very large reynolds numbers, Dokl. Akad. Nauk SSSR **30**, 9 (1941) [reprinted in *Proc. R. Soc. Lond. A* **434**, 9 (1991)].

- [2] U. Frisch, *Turbulence: The Legacy of A. N. Kolmogorov* (Cambridge University Press, Cambridge, UK, 1995).
- [3] Y. Zhou, Turbulence theories and statistical closure approaches, *Phys. Rep.* **935**, 1 (2021).
- [4] A. Alexakis and L. Biferale, Cascades and transitions in turbulent flows, *Phys. Rep.* **767-769**, 1 (2018).
- [5] G. Boffetta and R. E. Ecke, Two-dimensional turbulence, *Annu. Rev. Fluid Mech.* **44**, 427 (2012).
- [6] G. K. Batchelor, Computation of the energy spectrum in homogeneous two-dimensional turbulence, *Phys. Fluids* **12**, II-233 (1969).
- [7] R. H. Kraichnan, Inertial ranges in two-dimensional turbulence, *Phys. Fluids* **10**, 1417 (1967).
- [8] C. E. Leith, Diffusion approximation for two-dimensional turbulence, *Phys. Fluids* **11**, 671 (1968).
- [9] G. Boffetta, A. Celani, and M. Vergassola, Inverse energy cascade in two-dimensional turbulence: Deviations from Gaussian behavior, *Phys. Rev. E* **61**, R29(R) (2000).
- [10] D. Hurst and J. Vassilicos, Scalings and decay of fractal-generated turbulence, *Phys. Fluids* **19**, 035103 (2007).
- [11] K. Nagata, Y. Sakai, T. Inaba, H. Suzuki, O. Terashima, and H. Suzuki, Turbulence structure and turbulence kinetic energy transport in multiscale/fractal-generated turbulence, *Phys. Fluids* **25**, 065102 (2013).
- [12] R. Seoud and J. Vassilicos, Dissipation and decay of fractal-generated turbulence, *Phys. Fluids* **19**, 105108 (2007).
- [13] S. Laizet and J. C. Vassilicos, DNS of fractal-generated turbulence, *Flow, Turbul. Combust.* **87**, 673 (2011).
- [14] B. Mazzi and J. C. Vassilicos, Fractal-generated turbulence, *J. Fluid Mech.* **502**, 65 (2004).
- [15] F. P. Bretherton and D. B. Haidvogel, Two-dimensional turbulence above topography, *J. Fluid Mech.* **78**, 129 (1976).
- [16] G. K. Vallis and M. E. Maltrud, Generation of mean flows and jets on a beta plane and over topography, *J. Phys. Oceanogr.* **23**, 1346 (1993).
- [17] S. J. Benavides and A. Alexakis, Critical transitions in thin layer turbulence, *J. Fluid Mech.* **822**, 364 (2017).
- [18] K. Seshasayanan, S. J. Benavides, and A. Alexakis, On the edge of an inverse cascade, *Phys. Rev. E* **90**, 051003(R) (2014).
- [19] P. D. Mininni, D. Rosenberg, R. Reddy, and A. Pouquet, A hybrid MPI–OpenMP scheme for scalable parallel pseudospectral computations for fluid turbulence, *Parallel Comput.* **37**, 316 (2011).
- [20] H. Triebel, *Fractals and Spectra: Related to Fourier Analysis and Function Spaces* (Springer, Berlin, 2010).
- [21] K. Falconer, *Fractal Geometry: Mathematical Foundations and Applications* (Wiley, Hoboken, NJ, 2004).
- [22] J. C. Vassilicos, Dissipation in turbulent flows, *Annu. Rev. Fluid Mech.* **47**, 95 (2015).
- [23] R. Benzi, S. Ciliberto, R. Tripiccone, C. Baudet, F. Massaioli, and S. Succi, Extended self-similarity in turbulent flows, *Phys. Rev. E* **48**, R29(R) (1993).